Non-reciprocal Synchronization in Thermal Rydberg Ensembles

Yunlong Xue(薛云龙)[1] and Zhengyang Bai(白正阳)[2*]

[1]*State Key Laboratory of Precision Spectroscopy, East China Normal University, Shanghai 200062, China*
[2]*National Laboratory of Solid State Microstructures and School of Physics, Collaborative Innovation Center of Advanced Microstructures, Nanjing University, Nanjing 210093, China*

(Received 9 October 2025; accepted manuscript online 24 November 2025)

Optical non-reciprocity is a fundamental phenomenon in photonics. It is crucial for developing devices that rely on directional signal control, such as optical isolators and circulators. However, most research in this field has focused on systems in equilibrium or steady states. In this work, we demonstrate a room-temperature Rydberg atomic platform where the unidirectional propagation of light acts as a switch to mediate time-crystalline-like collective oscillations through atomic synchronization. We find that thermal-motion-induced coupling asymmetry, enabled by counter-propagating probe and control fields, generates persistent oscillations; conversely, co-propagation quenches this effect. We identify, through both numerical and analytical approaches, the criteria for realizing optical non-reciprocity within a synchronization regime. These results provide key insights for chiral quantum optics and promote the on-chip integration of non-reciprocal devices in nonequilibrium many-body systems.

DOI: 10.1088/0256-307X/43/1/010302 CSTR: 32039.14.0256-307X.43.1.010302

1. Introduction. Non-reciprocal optical components are cornerstones of modern photonic chips and quantum information networks.[1–10] Traditional implementations have been mainly dependent on magneto-optical effects,[11,12] whereas recent advances have expanded to emerging areas such as nonlinear and quantum optics.[8,13–16] A particularly promising approach utilizes the light propagation direction itself as a switching degree to control macroscopic responses.[17–19] In thermal atomic vapors, it has been demonstrated that a unidirectional control field, through interaction with atomic thermal motion, induces susceptibility–momentum locking via the Doppler effect, yielding pronounced steady-state non-reciprocity.[14,15] This strategy effectively harnesses thermal motion as a resource. It exploits direction-dependent light–matter interactions to break optical symmetry, thereby enabling precisely controllable responses.

A natural question arises as to whether such direction-dependent control mechanisms can also manipulate the dynamics of optical fields in nonequilibrium states and facilitate chiral switching in quantum many-body systems.[20–25] Exploring these chiral nonequilibrium effects demands an optical medium capable of sustaining strong and tunable light–matter interactions. Rydberg atomic gases inherently satisfy this requirement. When excited to high-lying Rydberg states, atoms exhibit strong dipole–dipole interactions, effectively converting the ensemble into a highly correlated quantum many-body medium.[26–29] These interactions give rise to rich many-body phenomena, such as antiferromagnetic phases,[26,30,31] quantum scars,[32,33] and many-body synchronization.[22,23]

In this work, we propose a theoretical scheme for achieving optical non-reciprocity in nonequilibrium states using thermal Rydberg ensembles. Our results show that in the counter-propagating configuration, atoms with different velocities synchronize via Rydberg interactions, leading to oscillatory dynamical phases characterized by frequency and phase locking in a subset of atoms. Conversely, both synchronization and the ensuing phases are suppressed under co-propagation. This establishes a direct link between optical non-reciprocity and nonequilibrium phases, thereby enabling the optical propagation direction to act as a switch for quantum dynamical states. Beyond its fundamental applications, the ability to operate at room temperature paves the way for designing and realizing practical nonequilibrium quantum optics devices.

2. Model. We consider an ensemble of three-level Rydberg atoms driven by external probe and coupling fields, as illustrated in Figs. 1(a2) and 1(b2). Atoms comprise a ground state $|g\rangle$, an intermediate excited state $|e\rangle$, and a highly excited Rydberg state $|r\rangle$. After applying a transformation to the rotating frame with respect to the free Hamiltonian and making the rotating-wave approximation, the atom–light interaction Hamiltonian takes the following form ($\hbar = 1$):

$$\begin{aligned}\hat{H}_{\rm ap} = & -\Delta_{\rm p}\hat{\sigma}_{\rm ee} - (\Delta_{\rm p}+\Delta_{\rm c})\hat{\sigma}_{\rm rr} \\ & + \frac{1}{2}(\Omega_{\rm p}\hat{\sigma}_{\rm eg} + \Omega_{\rm c}\hat{\sigma}_{\rm re} + {\rm H.c.}),\end{aligned} \tag{1}$$

where $\hat{\sigma}_{\alpha\beta}$ are atomic transition operators ($\alpha, \beta \in \{{\rm g}, {\rm e}, {\rm r}\}$). Here, $\Omega_{\rm p}$ and $\Omega_{\rm c}$ represent the Rabi frequencies

*Corresponding author. Email: zhybai@nju.edu.cn
© 2026 Chinese Physical Society and IOP Publishing Ltd. All rights, including for text and data mining, AI training, and similar technologies, are reserved.

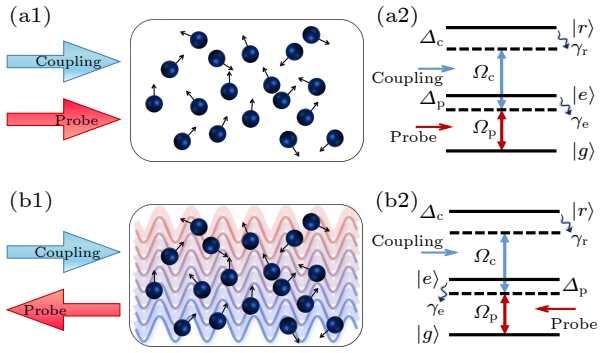

Fig. 1. Schematic diagram of the optical non-reciprocal synchronization model. (a1) and (b1) Schematics of the system response under co- and counter-propagating probe and coupling fields, respectively. (a2) and (b2) The corresponding energy-level diagram of the three-level Rydberg atom for each configuration.

of the probe and coupling lasers, respectively, while Δ_p and Δ_c denote their corresponding detunings.

$$\hat{H}_{\rm int} = -\mathcal{N}\int \mathrm{d}^3\boldsymbol{r}'\hat{\sigma}_{\rm rr}(\boldsymbol{r}',t)V_{\rm rr}(\boldsymbol{r}-\boldsymbol{r}')\hat{\sigma}_{\rm rr}(\boldsymbol{r},t). \tag{2}$$

Typically, the interaction between Rydberg atoms at positions $\boldsymbol{r}$ and $\boldsymbol{r}'$ is described by the van der Waals potential $V_{\rm rr}(\boldsymbol{r}-\boldsymbol{r}') = C_6/|\boldsymbol{r}-\boldsymbol{r}'|^6$, where C_6 is the dispersion coefficient, and $\mathcal{N}$ denotes the atomic density.

The system is described microscopically using a quantum master equation for the density operator $\hat{\rho}$,

$$\begin{aligned}\frac{\mathrm{d}\hat{\rho}}{\mathrm{d}t} =& -\mathrm{i}[\hat{H},\hat{\rho}]\\ &+\mathcal{N}\sum_{\alpha=\mathrm{r,e}}\gamma_\alpha\int \mathrm{d}^3\boldsymbol{r}\Big(\hat{L}_\alpha\hat{\rho}\hat{L}_\alpha^\dagger - \frac{1}{2}\{\hat{L}_\alpha^\dagger\hat{L}_\alpha,\hat{\rho}\}\Big),\end{aligned} \tag{3}$$

where the Hamiltonian $\hat{H}$ responsible for the coherent dynamics reads $\hat{H} = \mathcal{N}\int \mathrm{d}^3\boldsymbol{r}[\hat{H}_{\rm ap}(\boldsymbol{r},t) + \hat{H}_{\rm int}(\boldsymbol{r},t)]$. The second term on the right-hand side of Eq. (3) describes the dissipation process. In the Lindblad term, the operator $\hat{L}_{\rm r} = \hat{\sigma}_{\rm er}(\boldsymbol{r},t)$ and $\hat{L}_{\rm e} = \hat{\sigma}_{\rm ge}(\boldsymbol{r},t)$ corresponds to the transition $|r\rangle \to |e\rangle$ and $|e\rangle \to |g\rangle$ with the decay rates $\gamma_{\rm r}$ and $\gamma_{\rm e}$. The anticommutator is defined as $\{\hat{A},\hat{B}\} = \hat{A}\hat{B}+\hat{B}\hat{A}$.

Due to the dissipative nature of the Rydberg ensemble, mean-field (MF) theory can be employed to characterize the dynamical behavior of the system. Within this approximation, the many-body density matrix is decoupled into a product of single-particle matrices, which effectively neglects spatial correlations between different sites. This approximation adequately captures the dynamical behavior of the system as it approaches the thermodynamic limit, and provides a good description in high dimensions, where fluctuations from neighboring sites tend to average out.[34,35]

Starting from the Lindblad master Eq. (3), we derive the optical Bloch equations for the density matrix elements $\rho_{\alpha\beta}(\boldsymbol{r},t) \equiv \langle\hat{\sigma}_{\alpha\beta}(\boldsymbol{r},t)\rangle$, for example, the population dynamics are

$$\frac{\mathrm{d}\rho_{\rm gg}}{\mathrm{d}t} = \gamma_{\rm e}\rho_{\rm ee} - \tfrac{\mathrm{i}}{2}(-\Omega_{\rm p}\rho_{\rm ge} + \Omega_{\rm p}\rho_{\rm eg}), \tag{4a}$$

$$\frac{\mathrm{d}\rho_{\rm ee}}{\mathrm{d}t} = -\gamma_{\rm e}\rho_{\rm ee} + \gamma_r\rho_{\rm rr} - \tfrac{\mathrm{i}}{2}[\Omega_{\rm p}(\rho_{\rm ge}-\rho_{\rm eg}) + \Omega_{\rm c}(\rho_{\rm re}-\rho_{\rm er})], \tag{4b}$$

$$\frac{\mathrm{d}\rho_{\rm rr}}{\mathrm{d}t} = -\gamma_{\rm r}\rho_{\rm rr} - \tfrac{\mathrm{i}}{2}(\Omega_{\rm c}\rho_{\rm er} - \Omega_{\rm c}\rho_{\rm re}), \tag{4c}$$

$$\frac{\mathrm{d}\rho_{\rm ge}}{\mathrm{d}t} = d_{\rm ge}\rho_{\rm ge} - \tfrac{\mathrm{i}}{2}(-\Omega_{\rm p}\rho_{\rm gg} - \Omega_{\rm c}\rho_{\rm gr} + \Omega_{\rm p}\rho_{\rm ee}), \tag{4d}$$

$$\frac{\mathrm{d}\rho_{\rm gr}}{\mathrm{d}t} = d_{\rm gr}\rho_{\rm gr} - \tfrac{\mathrm{i}}{2}(-\Omega_{\rm c}\rho_{\rm ge} + \Omega_{\rm p}\rho_{\rm er}) - \mathrm{i}\overline{V}_{\rm rr}\rho_{\rm rr}^b\rho_{\rm gr}, \tag{4e}$$

$$\frac{\mathrm{d}\rho_{\rm er}}{\mathrm{d}t} = d_{\rm er}\rho_{\rm er} - \tfrac{\mathrm{i}}{2}(\Omega_{\rm p}\rho_{\rm gr} - \Omega_{\rm c}\rho_{\rm ee} + \Omega_{\rm c}\rho_{\rm rr}) - \mathrm{i}\overline{V}_{\rm rr}\rho_{\rm rr}^b\rho_{\rm er}, \tag{4f}$$

where $d_{\alpha\beta} = \mathrm{i}(\Delta_\alpha - \Delta_\beta) - \gamma_{\alpha\beta}$, with $\gamma_{\alpha\beta} \equiv (\gamma_\alpha + \gamma_\beta)/2$, $\Delta_{\rm e} = \Delta_{\rm p}$, $\Delta_{\rm r} = \Delta_{\rm p} + \Delta_{\rm c}$, $\Delta_{\rm g} = 0$, and $\overline{V}_{\rm rr}$ represents the effective MF interaction strength. In Eqs. (4e) and (4f), we introduce a MF shift of the Rydberg level that depends on the Rydberg density via a power law, $\overline{V}_{\rm rr}\rho_{\rm rr}^b$, parameterized by an exponent b. This dependence arises because Rydberg atoms interact via a power-law potential. Within the MF theory, this leads to an effective shift of the Rydberg level that scales with the density as $\rho_{\rm rr}^b$.[23]

Importantly, the steady-state solutions of Eq. (4) are not always unique due to the nonlinearity induced by Rydberg interactions. We characterize the phases using the Rydberg population $\rho_{\rm rr}$ as an order parameter.

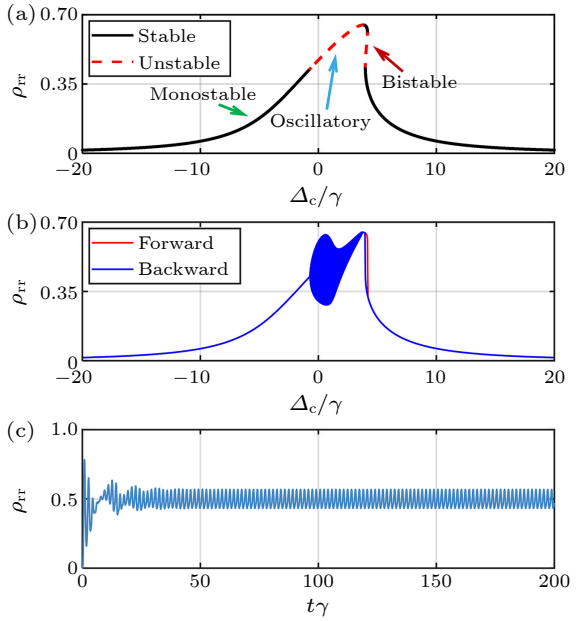

Fig. 2. The stability analysis and its dynamical simulation. (a) As detuning $\Delta_{\rm c}$ is varied, the system is partitioned into three distinct regimes based on the number and stability of fixed points: monostable, bistable, and oscillatory. (b) We adiabatically sweep the $\Delta_{\rm c}$ in both directions to measure the values of $\rho_{\rm rr}$. (c) Time dynamics of $\rho_{\rm rr}$ in the oscillatory regime at $\Delta_{\rm c} = 0$. Simulation parameters are set as follows: $b = 2$, $\gamma_{\rm e} = \gamma = 1$, $\gamma_{\rm r} = 10^{-3}\gamma$, $\Delta_{\rm p} = 0$, $\overline{V}_{\rm rr} = -9\gamma$, $\Omega_{\rm c} = 4.4\gamma$, and $\Omega_{\rm p} = 6\gamma$.

Through linear stability analysis around the fixed points, three characteristic dynamical regimes are identified: the monostable phase, which has a single stable steady state; the bistable phase, characterized by two coexisting stable solutions; and the oscillatory phase, in which no stable stationary fixed point exists [Fig. 2(a)].

To probe the dynamical phase of the system, we sweep the detuning Δ_c adiabatically from large positive to large negative values, and vice versa [Fig. 2(b)]. Near resonance, the system exhibits rapid oscillations due to the absence of stable fixed points. This interplay between driving and dissipation drives the system into a time-crystalline phase.[21] Within the bistable regime, the forward and backward sweeps follow distinct trajectories, resulting in a hysteresis loop.[35]

Physically, the transition from the monostable to the bistable phase stems from the interplay between coherent driving and nonlinear Rydberg interactions, whereas the oscillatory regime arises when this competition destabilizes all stationary solutions. Remarkably, the time-crystalline phase of interest here naturally arises within this non-stationary regime, where the system maintains persistent oscillations in the absence of any stable steady state. As shown in Fig. 2(c), this is accompanied by a breaking of time-translation symmetry, dynamically manifested as sustained and undamped oscillations.

3. Non-reciprocal Synchronization. Inspired by the oscillatory dynamics observed in Rydberg systems, we will extend our research to room-temperature (or thermal) Rydberg gases. This will allow us to study synchronization among atoms belonging to different velocity classes and pursue optical non-reciprocity in nonequilibrium states.

To simulate the dynamics in thermal atomic systems, Doppler shifts arising from atomic motion are accounted for: atoms with velocity v experience modified detunings $\Delta_\alpha \to \Delta_\alpha + \boldsymbol{k}_\alpha \cdot \boldsymbol{v}$ for $\alpha = \mathrm{p}, \mathrm{c}$, where $\boldsymbol{k}_\mathrm{p}$ ($\boldsymbol{k}_\mathrm{c}$) is the wave vector of the probe (coupling) field. Assuming the system is in thermal equilibrium, only the velocity component parallel to the direction of laser propagation contributes to the Doppler effect, while the perpendicular components do not. This reduces the velocity field from a three-dimensional problem to a one-dimensional one. As a result, the atomic velocities follow a one-dimensional Maxwell–Boltzmann distribution given by $f(v) = \frac{1}{\sqrt{\pi} v_{T_\mathrm{c}}} \exp[-(v/v_{T_\mathrm{c}})^2]$, where $v_{T_\mathrm{c}} = \sqrt{2k_\mathrm{B}T_\mathrm{c}/M}$ is the most probable speed at temperature T_c, and M denotes the atomic mass. Then, the macroscopic response can be obtained by thermal averaging over velocity-dependent density matrix elements $\tilde{\rho}_{\alpha\beta} = \int \mathrm{d}v\, f(v)\rho_{\alpha\beta}(v)$.

Such Doppler broadening is a common feature in room-temperature atomic gas experiments and typically averages out nontrivial dynamical features in conventional quantum many-body systems, making them effectively undetectable in macroscopic measurements. However, in our system, atoms belonging to different velocity classes are nonlinearly coupled through MF interactions of the form $\int \mathrm{d}v f(v)\overline{V}_{\mathrm{rr}}\rho^b_{\mathrm{rr}}(v)\rho_{\alpha\beta}(v)$ ($\alpha \neq \beta$; $\alpha, \beta = \mathrm{g}, \mathrm{e}, \mathrm{r}$). As a result, the evolution of each velocity class is not independent of the others. This is the essential element of the atomic synchronization mechanism.[23,36]

Moverover, nonreciprocity in such system also emerges when atomic thermal motion is taken into account. The direction-dependent microscopic Doppler effect alters the effective two-photon detuning $\Delta_\mathrm{p} + \Delta_\mathrm{c}$. Thus, the light–atom interaction described by Hamiltonian (1) becomes asymmetric, leading to a chiral atomic response.[15] When the probe and control laser beams counter-propagate, the Doppler shifts experienced by moving atoms have opposite signs. Consequently, their contributions to the two-photon detuning, $\Delta_\mathrm{p} + \Delta_\mathrm{c} - (k_\mathrm{p} - k_\mathrm{c})v$, partially cancel each other out. This configuration places the system in a synchronized regime, enabling the observation of persistent oscillations in the transmission signal. In contrast, when the two beams are co-propagating, the Doppler shifts share the same sign. This amplifies their impact on the two-photon detuning, now given by $\Delta_\mathrm{p} + \Delta_\mathrm{c} - (k_\mathrm{p} + k_\mathrm{c})v$ which drives the system out of the oscillatory regime and into a stationary state.

As illustrated in Fig. 3(a1), we analyze the dynamical behavior of the system across different velocity classes, under counter-propagating probe and coupling fields. It is found that dynamics of atoms with different velocity classes are largely different during the initial transient period. At a later stage ($t\gamma > 200$), we observe the emergence of synchronization as a significant fraction of atoms with negative velocity ($v < 0$; see the blue curve) are attracted toward a limit cycle, where they begin to oscillate with a common frequency and fixed phase relationship. As more velocity classes become phase-locked, the MF strength increases. This, in turn, drives additional velocity classes to align their oscillations, ultimately leading to a partially or fully synchronized state. In the simulation, we generate 150 groups of atoms with distinct velocities, whose statistical weights are shown in Fig. 3(c) and follow a Maxwell–Boltzmann distribution. The interaction density term is updated iteratively at each time step.

After Doppler averaging, the emergence of atomic synchronization leads to persistent, time-periodic oscillations in the optical transmission as the system evolves toward a nonequilibrium steady state [Fig. 3(a2)]. This behavior represents a hallmark signature of the spontaneous breaking of temporal translational symmetry. The optical transmission is given by $T = \exp[-k_\mathrm{p}\mathrm{Im}(\chi_\mathrm{p})L]$, where the susceptibility $\chi_\mathrm{p} = 2\mathcal{N}|\mu_{\mathrm{eg}}|^2 \int \mathrm{d}v f(v)\rho_{\mathrm{ge}}(v)/[\varepsilon_0\Omega_\mathrm{p}]$ integrates over the velocity distribution. Here, μ_{eg} denotes the dipole moment between the ground and excited states, and L is the length of the optical medium. Therefore, the emergence of macroscopic oscillations in the optical response of a hot Rydberg vapor is a manifestation of a Kuramoto-like synchronization transition,[37,38] which is driven by sufficiently strong Rydberg interactions. Such synchronized oscillations correspond to the oscillatory dynamics recently observed in experiments.[21–23]

However, under co-propagating illumination with a reversed incidence direction, atoms across the velocity distribution exhibit a conventional dynamical response [Figs. 3(b1) and 3(b2)]. The optical transmission undergoes rapid transient oscillations prior to settling into

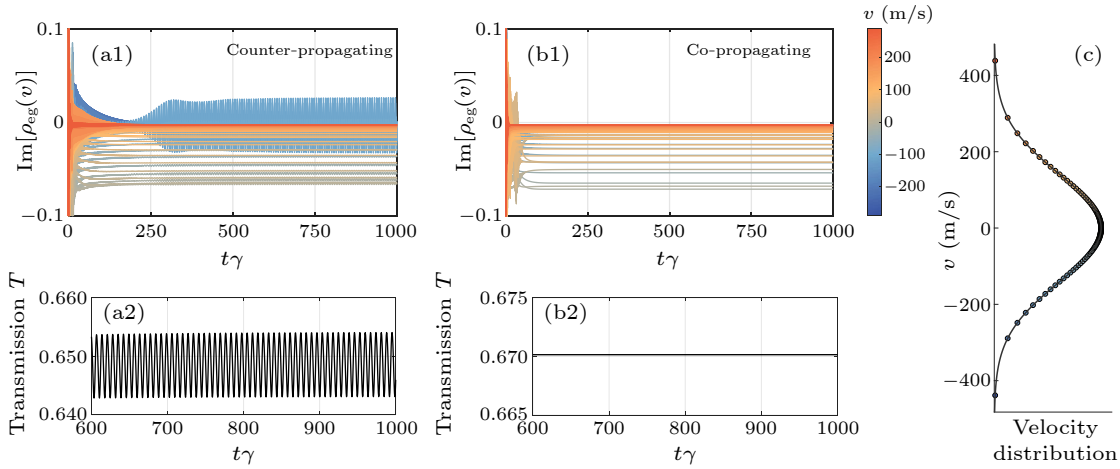

Fig. 3. Non-reciprocal synchronization dynamics. (a1) and (b1) Dynamics of $\mathrm{Im}[\rho_{\mathrm{eg}}(v)]$ for atomic velocities between -400 m/s and 400 m/s under the counter-propagating (co-propagating) condition. (a2) and (b2) Dynamics of transmission T under co-propagating (counter-propagating) conditions after Doppler averaging. (c) The velocities of the 150 atomic groups used in the simulation are initialized by sampling from the Maxwell–Boltzmann distribution at a temperature of $T_{\mathrm{c}} = 321$ K. Simulation parameters are set as follows: $\Omega_{\mathrm{p}} = 6\gamma$, $\Omega_{\mathrm{c}} = 4\gamma$, $\Delta_{\mathrm{p}} = 0$, $\Delta_{\mathrm{c}} = -11\gamma$, and $\overline{V}_{\mathrm{rr}} = -800\gamma$.

a steady state. This stands in sharp contrast to the synchronized behavior seen in Figs. 3(a1) and 3(a2). Notably, chiral coupling is induced by atomic thermal motion. This coupling causes the system to exhibit markedly different dynamical responses under distinct propagation conditions, thereby realizing a non-reciprocal synchronized state.

Similar to the Kuramoto model,[23,38] a time-crystal phase emerges via synchronization among atoms of different velocity classes. The synchronization is governed by each group's intrinsic frequency, the coupling strength, and the power and detuning of the driving fields. Crucially, the propagation direction of the laser field modifies the effective detuning distribution across velocity groups. This modification disrupts the synchronization parameters, thereby causing the different dynamics observed under different propagation directions.

We further test the robustness of this chiral dynamical response. This is a key criterion for assessing the potential of non-reciprocal quantum systems for operation across diverse parametric regimes. For fixed Rabi frequencies $\Omega_{\mathrm{p}} = 6\gamma$ and $\Omega_{\mathrm{c}} = 4\gamma$, we extract the oscillation frequencies (f_{cou}, f_{co}) and their amplitudes as a function of detuning Δ_{c} from the dynamical spectra for both counter- and co-propagating configurations, as summarized in Fig. 4. The counter-propagating configuration [Fig. 4(a)] sustains synchronized dynamics over a broad detuning range from -12.5γ to 4.7γ, a behavior markedly absent in the co-propagating case [Fig. 4(b)]. This demonstrates the robustness of the non-reciprocal dynamical response to parameter variations. In non-equilibrium systems, the information can be encoded on the oscillatory frequency of transmission. We quantify the optical non-reciprocity by the contrast ratio η, which is based on the oscillation frequencies and given by $\eta = (f_{\mathrm{cou}} - f_{\mathrm{co}})/(f_{\mathrm{cou}} + f_{\mathrm{co}})$. Since synchronization is perfectly suppressed under co-propagation (i.e., $f_{\mathrm{co}} = 0$), a contrast ratio $\eta = 100\%$ is

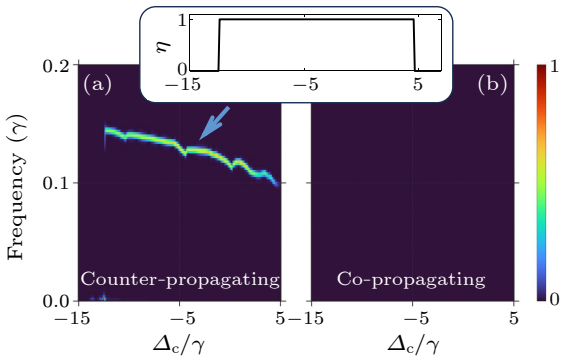

Fig. 4. Non-reciprocal synchronized response versus the detuning of the coupling field. (a) and (b) The oscillation frequencies of transmission under counter-propagating (co-propagating) condition. The color map represents the normalized oscillation amplitude. The simulation parameters are consistent with those in Fig. 3. The inset shows the contrast ratio η versus Δ_{c}.

achieved across a broad laser frequency range [see the inset of Fig. 4].

4. Conclusion and Discussion. In this work, we systematically explore non-reciprocal synchronization in a thermal Rydberg gas. Our core innovation is the introduction of motion-induced chirality, which generalizes optical non-reciprocity from the steady state to the dynamical, nonequilibrium regime,[10,15] demonstrating the formation of a chiral time crystal. The robustness of this phenomenon, demonstrated by its pronounced dynamics over a wide range of laser frequency, highlights its potential for non-equilibrium quantum device design. As shown in recent studies,[24,25,39] our work can be extended into the quantum regime using cavity-QED systems or Rydberg-atom arrays, opening the door to observing genuine quantum fluctuation synchronization and realizing a nonreciprocal quantum time crystal.[40] Such systems would not only be of fundamental interest but also hold promise for several frontier applications, including the design of nonreciprocal quantum devices,[2] and the development of

quantum precision measurement techniques.[41] Our findings thereby pave the way for engineering diverse nonreciprocal effects in driven-dissipative systems.

Acknowledgements. This work was supported by the National Natural Science Foundation of China (Grant No. 12274131) and the Innovation Program for Quantum Science and Technology (Grant No. 2024ZD0300101).

References

[1] Fruchart M, Hanai R, Littlewood P B, and Vitelli V 2021 *Nature* **592** 363
[2] Barzanjeh S, Xuereb A, Alù A, Mann S A, Nefedkin N, Peano V, and Rabl P 2025 arXiv:2508.03945
[3] Dutt A, Mohanty A, Gaeta A L, and Lipson M 2024 *Nat. Rev. Mater.* **9** 321
[4] Luo W, Cao L, Shi Y, Wan L, Zhang H, Li S, Chen G, Li Y, Li S, Wang Y, Sun S, Karim M F, Cai H, Kwek L C, and Liu A Q 2023 *Light Sci. Appl.* **12** 175
[5] Kim S, Sohn D B, Peterson C W, and Bahl G 2021 *APL Photonics* **6** 011301
[6] Luo K H, Brauner S, Eigner C, Sharapova P R, Ricken R, Meier T, Herrmann H, and Silberhorn C 2019 *Sci. Adv.* **5** eaat1451
[7] Sounas DL and Alù A 2017 *Nat. Photon.* **11** 774
[8] Shen Z, Zhang Y L, Chen Y, Zou C L, Xiao Y F, Zou X B, Sun F W, Guo G C, and Dong C H 2016 *Nat. Photon.* **10** 657
[9] Khanikaev AB and Alù A 2015 *Nat. Photon.* **9** 359
[10] Lodahl P, Mahmoodian S, Stobbe S, Rauschenbeutel A, Schneeweiss P, Volz J, Pichler H, and Zoller P 2017 *Nature* **541** 473
[11] Huang B, Cenker J, Zhang X, Ray E L, Song T, Taniguchi T, Watanabe K, McGuire M A, Xiao D, and Xu X 2020 *Nat. Nanotechnol.* **15** 212
[12] Feng W, Hanke J P, Zhou X, Guo G Y, Blügel S, Mokrousov Y, and Yao Y 2020 *Nat. Commun.* **11** 118
[13] Wang Z B, Zhang Y L, Hu X X, Chen G J, Li M, Yang P F, Zou X B, Zhang P F, Dong C H, Li G, Zhang T C, Guo G C, and Zou C L 2025 *Light Sci. Appl.* **14** 23
[14] Liang C, Liu B, Xu A N, Wen X, Lu C, Xia K, Tey M K, Liu Y C, and You L 2020 *Phys. Rev. Lett.* **125** 123901
[15] Zhang S, Hu Y, Lin G, Niu Y, Xia K, Gong J, and Gong S 2018 *Nat. Photon.* **12** 744
[16] Huang R, Miranowicz A, Liao J Q, Nori F, and Jing H 2018 *Phys. Rev. Lett.* **121** 153601
[17] Zola R S, Bisoyi H K, Wang H, Urbas A M, Bunning T J, and Li Q 2019 *Adv. Mater.* **31** 1806172
[18] Dorrah A H, Rubin N A, Zaidi A, Tamagnone M, and Capasso F 2021 *Nat. Photon.* **15** 287
[19] Jin L and Song Z 2018 *Phys. Rev. Lett.* **121** 073901
[20] Xie C, Sun K, Wu K D, Li C F, Guo G C, Yi W, and Xiang G Y 2025 *Sci. Bull.* **70** 3345
[21] Wu X, Wang Z, Yang F, Gao R, Liang C, Tey M K, Li X, Pohl T, and You L 2024 *Nat. Phys.* **20** 1389
[22] Ding D, Bai Z, Liu Z, Shi B, Guo G, Li W, and Adams C S 2024 *Sci. Adv.* **10** eadl5893
[23] Wadenpfuhl K and Adams C S 2023 *Phys. Rev. Lett.* **131** 143002
[24] Lai D G, Miranowicz A, and Nori F 2025 *Nat. Commun.* **16** 8491
[25] Nadolny T, Bruder C, and Brunelli M 2025 *Phys. Rev. X* **15** 011010
[26] Bernien H, Schwartz S, Keesling A, Levine H, Omran A, Pichler H, Choi S, Zibrov A S, Endres M, Greiner M, Vuletić V, and Lukin M D 2017 *Nature* **551** 579
[27] Adams C S, Pritchard J D, and Shaffer J P 2020 *J. Phys. B* **53** 012002
[28] Bendkowsky V, Butscher B, Nipper J, Shaffer JP, Löw R, and Pfau T 2009 *Nature* **458** 1005
[29] Saffman M, Walker T G, and Mølmer K 2010 *Rev. Mod. Phys.* **82** 2313
[30] Ebadi S, Wang T T, Levine H, Keesling A, Semeghini G, Omran A, Bluvstein D, Samajdar R, Pichler H, Ho W W, Choi S, Sachdev S, Greiner M, Vuletić V, and Lukin M D 2021 *Nature* **595** 227
[31] Guardado-Sanchez E, Brown P T, Mitra D, Devakul T, Huse D A, Schauß P, and Bakr W S 2018 *Phys. Rev. X* **8** 021069
[32] Turner C J, Michailidis A A, Abanin D A, Serbyn M, and Papić Z 2018 *Nat. Phys.* **14** 745
[33] Bluvstein D, Omran A, Levine H, Keesling A, Semeghini G, Ebadi S, Wang T T, Michailidis A A, Maskara N, Ho W W, Choi S, Serbyn M, Greiner M, Vuletić V, and Lukin M D 2021 *Science* **371** 1355
[34] Lee TE, Häffner H, and Cross M C 2011 *Phys. Rev. A* **84** 031402
[35] Carr C, Ritter R, Wade C G, Adams C S, and Weatherill K J 2013 *Phys. Rev. Lett.* **111** 113901
[36] Bai Z, Adams C S, Huang G, and Li W 2020 *Phys. Rev. Lett.* **125** 263605
[37] Kuramoto Y 1975 *Lect. Notes Phys.* **39** 420
[38] Acebrón J A, Bonilla L L, Pérez Vicente C J, Ritort F, and Spigler R 2005 *Rev. Mod. Phys.* **77** 137
[39] Zhang Z, Xu Z, Huang R, Lu X, Zhang F, Li D, Özdemir Ş K, Nori F, Bao H, Xiao Y, Chen B, Jing H, and Shen H 2025 *Nat. Photon.* **19** 840
[40] Russo F and Pohl T 2025 *Phys. Rev. Lett.* **135** 110404
[41] Cabot A, Carollo F, and Lesanovsky I 2024 *Phys. Rev. Lett.* **132** 050801